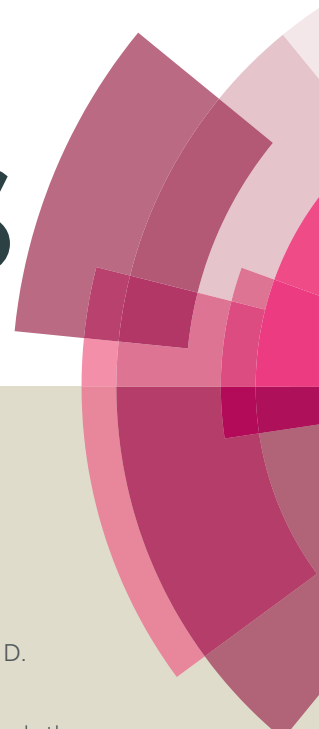


RSC Advances



This article can be cited before page numbers have been issued, to do this please use: A. Chakravarty, D. Sengupta, B. Basu, A. Mukherjee and G. De, *RSC Adv.*, 2015, DOI: 10.1039/C5RA17777D.



This is an *Accepted Manuscript*, which has been through the Royal Society of Chemistry peer review process and has been accepted for publication.

Accepted Manuscripts are published online shortly after acceptance, before technical editing, formatting and proof reading. Using this free service, authors can make their results available to the community, in citable form, before we publish the edited article. This *Accepted Manuscript* will be replaced by the edited, formatted and paginated article as soon as this is available.

You can find more information about *Accepted Manuscripts* in the [Information for Authors](#).

Please note that technical editing may introduce minor changes to the text and/or graphics, which may alter content. The journal's standard [Terms & Conditions](#) and the [Ethical guidelines](#) still apply. In no event shall the Royal Society of Chemistry be held responsible for any errors or omissions in this *Accepted Manuscript* or any consequences arising from the use of any information it contains.



RSC Advances

ARTICLE

MnO₂ Nanowires Anchored on Amine Functionalized Graphite Nanosheets: Highly Active and Reusable Catalyst for Organic Oxidation Reactions

Received 00th January 20xx,
Accepted 00th January 20xx

DOI: 10.1039/x0xx00000x

www.rsc.org/

A. Chakravarty,^a D. Sengupta,^b B. Basu,^{b*} A. Mukherjee^a and G. De^{a*}

A facile method of synthesizing MnO₂ nanowire on amine functionalized graphite nanosheet (AFGNS) has been accomplished. A probable mechanism has been proposed where the –NH₂ groups on AFGNS surface create a weakly basic environment assisting the reduction of KMnO₄ to MnO₂ nanoparticles followed by its anchoring and oriented growth to form MnO₂ nanowires. The as prepared MnO₂@AFGNS composite has been efficiently used as a selective heterogeneous catalyst for oxidation of primary and secondary benzyl alcohols to corresponding carbonyl compounds under aerobic condition in high yields in the absence of any other oxidizing or activating agent. While MnO₂ is considered as the most efficient and selective catalyst for the oxidation of benzyl and allyl alcohols, its large excess use (200 mol% with respect to the substrate) has been circumvented in this work by using heterogeneous AFGNS supported MnO₂ (only 7 mol% with respect to the substrate). The synergistic effect between the 1-D MnO₂ nanowire and AFGNS facilitates very fast e[–] transfer enabling such huge enhancement of the catalytic activity of the MnO₂@AFGNS composite. The composite also shows sufficient reuse capability and stability after 3 cycles of catalysis thus making it a potentially cheap and active catalyst in the field of organic catalysis.

1. Introduction

Oxidation of alcohol to carbonyl compound is a fundamental organic transformation from both synthetic and industrial points of view owing to the wide range application of the products as intermediates and precursors for several reaction systems.¹ For example, 4-methoxybenzaldehyde has high demand in food and perfume industries, as precursor for synthesis of drugs and UV-B agent and in metal plating with an estimated minimum global demand of 7000 tpa.² The simplest reaction pathway to satisfy such huge global demand of carbonyl compounds involves oxidation of their corresponding alcohols. Stoichiometric amount of high valent metal oxidants have been traditionally used to accomplish this transformation. But they have high toxicity and economic issues.³ For example, chromium and ruthenium-based reagents are toxic, irritants and corrosive. Manganese dioxide (MnO₂) being cost effective and environment-friendly has

been used over the years as a highly efficient and selective catalyst for oxidation of allylic and benzylic alcohols to aldehydes, amines to imines, oxidation of CO, H₂O₂ decomposition, oxygen reduction, oligomerization of methane and hydrogenolysis of propane.^{4–10}

MnO₂ exists in different crystallographic forms such as α, β and γ with 1-D tunnels in their structure, δ having layered 2-D structure and λ with a 3-D spinel structure. Their activity is also dependent on the different crystallographic structures due to the different types of interlinking of the MnO₆ octahedral units in the different polymorphs.¹¹ 1-D MnO₂ nanowires and nanorods have low dimensionality, high specific surface area, short diffusion paths for e[–] and tendency to facilitate redox reactions. They also show enhanced catalytic performance and have been the focus of intense investigations.¹² However, the low inherent electrical conductivity of MnO₂ hinders the process of e[–] transfer during catalysis thereby partially reducing their efficiency¹¹ and hence requiring large quantity of the reagent.

Graphite nanosheets (GNS) are 2-D graphite nanomaterials having a completely conjugated sp² hybridized framework with lateral thickness >5 nm.¹³ The planar structure of GNS with large surface area leads to increase in interfacial contact with metal oxide nanoparticles (NP). This coupled with the high electrical conductivity of GNS leads to increased charge transfer to the NP thus significantly enhancing catalytic performance of the NP making GNS an efficient catalyst support in heterogeneous catalytic system.^{13,14} Although graphite nanomaterials have been used as support for

^a Nano-Structured Materials Division, CSIR–Central Glass & Ceramic Research Institute, 196, Raja S. C. Mullick Road, Kolkata–700032, India. E-mail: gde@cgcrici.res.in

^b Department of Chemistry, North Bengal University, Darjeeling–734013, India. E-mail: basu_nbu@hotmail.com

*Electronic Supplementary Information (ESI) available: [FTIR spectrum of –NO₂ functionalized GNS (Fig. S1); XRD pattern and Raman spectrum of control reaction with microcrystalline graphite and MnO₂@AFGNS (Fig. S2); Table for oxidation of 4-methoxybenzyl alcohol using MnO₂@AFGNS catalyst with different loading of MnO₂ (Table S1); Reusability graph of MnO₂@AFGNS catalyst (Fig. S3); TEM image of MnO₂@AFGNS catalyst recovered after third cycle (Fig. S4)]. See DOI: 10.1039/x0xx00000x

synthesis of MnO₂ nanowires,^{15,16} the application of their composite is limited as anode materials in lithium ion batteries,¹⁷ with very few reports of their use as catalyst in organic reactions. Only recently, MnO₂ nanorods–graphene oxide (GO) composite has been successfully used as an active and cheap heterogeneous catalyst for the synthesis of amides from alcohol and amines and conversion of aromatic amines to azo compounds.^{16,18}

Synthesis of 1-D nanowires by the oriented growth of MnO₂ NP generally require soft template, solid template or patterned catalyst to acquire the desired nano-architecture, which makes the process arduous.^{19,20} A self seeded method of synthesis of MnO₂ nanowire is always more desirable for large scale production. Again, oxidation of graphite and graphene to create functional groups on their surface is imperative in anchoring of the MnO₂ NP with homogeneous distribution.^{21,22} The most common methods for synthesis MnO₂ nanowire GO/graphite/graphene composite includes co-precipitation in the presence of MnCl₂ and KMnO₄,^{16,21} hydrothermal process,^{15,23–25} electrochemical deposition,²⁶ high temperature reflux,²⁷ and solution phase assembly of graphene sheets and MnO₂ nanowires.²⁸ But there are some drawbacks related to GO such as its nearly insulating graphitic framework, which is incompletely regained on reduction to RGO with concomitant loss of functional groups.²⁴ This leads to aggregation of NP on their surface affecting their catalytic efficiency on reuse.²⁹ Alternative route for controlled chemical functionalization of GNS with lesser damage to the graphitic framework is thus essential presently. Interestingly, amine (–NH₂) group is effective in anchoring metal and metal oxide NP,³⁰ and recently we have reported synthesis of Cu₂O–amine functionalized GNS (AFGNS) composite where –NH₂ group has been successfully used for anchoring and stabilizing Cu₂O NP at room temperature.¹³

In connection with our interest in this potential field of material sciences and subsequent applications in organic catalysis we presumed that combination of the inherent low electron transfer ability of MnO₂ and high electron conductor AFGNS might give rise to a nanocomposite, which would exhibit enhanced catalytic activity in the oxidation process and thus avoiding the large excess use of MnO₂. During the synthesis of MnO₂ nanowire, the AFGNS matrix creates a basic environment which facilitates the reduction of KMnO₄ to MnO₂ NP. The –NH₂ functional groups on AFGNS surface also help to anchor MnO₄[–] and subsequently stabilize the MnO₂ NP, which undergoes an oriented growth to form nanowire structure. The as prepared composite exhibits high catalytic efficiency in the oxidation of primary and secondary benzyl alcohols to corresponding carbonyl compounds in aerobic condition. To the best of our knowledge, such organic oxidation reaction with MnO₂–functionalized GNS composite has not yet been explored. It is noteworthy here that the MnO₂@AFGNS catalyst is selective towards oxidation of primary alcohol to aldehyde, not giving any further oxidized product. Moreover, the oxidation reaction in presence of MnO₂@AFGNS does not require any other oxidizing agents such as peroxides and molecular O₂^{31,32} or activating agents

such as inorganic bases in the reaction medium unlike in case of other MnO₂ based catalysts used for this purpose.^{33,34} Further, the molar equivalent of MnO₂ with respect to alcohol substrate used for the oxidation reaction by MnO₂@AFGNS was distinctly lower compared to the other supported MnO₂ catalyst system^{33–36} thus making MnO₂@AFGNS ideal for large scale industrial application. The AFGNS matrix makes the catalyst easily separable and the reusability capacity of the composite was found to be sufficiently high even up to 3 cycles. Oxidation of benzyl amine to corresponding imine and aldehyde was also carried out with MnO₂@AFGNS to explore the versatility of the composite towards application in organic catalysis. The material being cost effective with facile method of preparation can have large scale application as highly efficient active reusable catalyst in the field of catalytic organic processes.

2. Experimental Section

2.1 Materials

The following chemicals were used as received: graphite powder (<20 µm, synthetic), KMnO₄, benzyl alcohol and other chemicals were purchased from Sigma–Aldrich, India. Na₂S (purified), H₂SO₄ (36 N), HNO₃ (16 N) were supplied by Merck. For column chromatography, silica (60–120 mm) (SRL, India) was used. For thin layer chromatography (TLC) plates (Merck) coated with silica gel 60, F₂₅₄ were used and 0.22 µm poly(vinylidene fluoride) (PVDF) membrane was purchased from Millipore. High pure water (18 MΩ) was obtained from a Milli–Q system (Millipore).

2.2 Characterization

High angle X–ray diffraction (XRD) measurements of the powders were performed with a Rigaku SmartLab X–ray diffractometer operating at 9 kW (200 mA; 45 kV) using Cu–Kα radiation. Fourier transform infrared (FTIR) absorption spectra of the samples were recorded using a Nicolet 380 FTIR spectrophotometer by KBr pellet method. Raman spectra were obtained using a Renishaw In Via reflex micro Raman spectrometer with excitation of argon ion (514 nm) lasers. The resolution was 1 cm^{–1} and sufficiently low laser power was used in order to avoid heating of the samples. X–ray photoelectron spectroscopy (XPS) measurements were done on a PHI 5000 Versaprobe II XPS system with Al Kα source and a charge neutralizer at room temperature, maintaining a base pressure about 6 × 10^{–10} mbar and energy resolution of 0.6 eV. High–resolution scans of Mn 2p, O 1s, C 1s, and N 1s were taken. At least two separate locations were analyzed for each sample. The concentrations of Mn in the composites have been estimated by inductively coupled plasma atomic emission spectroscopy (ICP–AES) using Spectro Ciros Vision, Germany. The average Mn content of the composites was determined from three different sets of composite samples of different weights. For the sample preparation for ICP analysis, a precisely weighed amount of the composite (4.5 mg) was treated at 950 °C for 5 h to remove the graphitic particles. The residue was digested with 6 mL of aqua regia in a Teflon

container and evaporated to dryness at 50 °C. The process was repeated 3 times each with 3 mL of aqua regia. The solid residue obtained finally was dissolved in 5 vol % of aqueous HNO₃ in a 250 mL volumetric flask. Finally this solution was used for the estimation of Mn by ICP analysis. The same experiment was repeated using 3.9 and 5.5 mg sample. Transmission electron microscope (TEM) measurements were carried out with JEOL JEM 2100F operating at 200 kV. Field emission scanning electron microscope (FESEM) measurements were carried out using a ZEISS SUPRA 35 VP FESEM. ¹H and ¹³C NMR spectra were taken in CDCl₃ using Bruker Avance AV-300 spectrometer operating at 300 MHz and 75 MHz respectively. Chemical shifts are reported in ppm with the solvent resonance as the internal standard (CDCl₃: δ 77.00 ppm).

2.3 Synthesis of amine functionalized graphite nanosheet (AFGNS)

The synthesis was done following our previously reported method.³⁷ For synthesis of AFGNS, initially 200 mg of microcrystalline graphite powder was ultrasonicated with 200 mL of 1:1 (v/v) mixed H₂SO₄ (36 N) and HNO₃ (16 N) in an ultrasonic bath for 30 min and then stirring at 25 °C for 24 h for synthesis of –NO₂ functionalized GNS. The solution was then quenched in 1 L of distilled water and filtered through 0.22 μm PVDF membrane and washed until the filtrate reached neutral pH. The residue thus obtained was dried overnight in vacuum. For synthesis of –NH₂ groups, 100 mg of the –NO₂ functionalized GNS sample was dispersed in 30 mL of distilled water and sonicated in an ultrasonic bath for 45 min. Then 1.5 g of Na₂S was added to the mixture and refluxed at 160 °C for 24 h. The product was filtered through 0.22 μm PVDF membrane and thoroughly washed with 250 mL of distilled water to remove the excess Na₂S and the other by products formed during the reaction. This AFGNS powder thus obtained was then dried in vacuum and collected.

2.4 Synthesis of MnO₂@AFGNS composite

For the synthesis of MnO₂ nanowire on AFGNS support, 30 mg AFGNS was homogeneously dispersed in 42.5 mL distilled water by ultrasonication for 30 min in an ultrasonic bath. Correspondingly, KMnO₄ (35 mg, 2.2 × 10^{−4} mol) was dissolved in distilled water (42.5 mL) in a round-bottom flask. To the aqueous dispersion of AFGNS, KMnO₄ solution was then added dropwise slowly under continuous stirring. After complete mixing, the mouth of the round-bottom flask was fitted with a cork and the solution was kept at 80 °C under stirring condition. After 48 h the solution was filtered, washed thoroughly with distilled water and the MnO₂@AFGNS composite thus obtained was dried in vacuum. From ICP analysis composition of the composite was determined. It was found that 7.6 wt % MnO₂ was present in MnO₂@AFGNS composite.

2.5 Representative procedure for the oxidation of benzyl alcohol

A mixture of 4-methoxybenzyl alcohol (0.5 mmol), MnO₂@AFGNS (40 mg, 0.035 mmol equivalent MnO₂) in 1,4-dioxane (3 mL) was heated at 100 °C with gentle magnetic stirring under aerobic condition. The progress of the reaction was monitored by checking TLC and after 12 h it was observed that the 4-methoxybenzyl alcohol was completely consumed. The reaction mixture was cooled, diethyl ether (5 mL) was added, centrifuged and the supernatant liquid was separated. The process was repeated thrice and the combined organic layer was concentrated under vacuum to afford an oily residue, which was purified through column chromatography over silica gel and elution with 4% ethyl acetate–light petroleum to furnish 4-methoxybenzaldehyde as colourless liquid,³⁸ (56 mg, 82%); ¹H NMR (CDCl₃, 300 MHz): δ/ppm 3.89 (s, 3H, OCH₃), 7.00 (dd, *J* = 1.8 and 6.6 Hz, 2H, ArH), 7.84 (dd, *J* = 1.8 and 6.6 Hz, ArH), 9.88 (s, 1H, CHO); ¹³C NMR (CDCl₃, 75 MHz): δ/ppm 55.5, 114.2, 129.8, 131.9, 164.5, 190.8. All other related products were characterized by comparison with respective literature data, like m.p. and/or NMR–spectral data.

2.6 Procedure for the oxidation of benzyl amine

A mixture of benzyl amine (1 mmol), MnO₂@AFGNS (40 mg, 0.035 mmol equivalent MnO₂) in 1,4-dioxane (3 mL) was heated at 100 °C for 12 h with gentle magnetic stirring under aerobic condition. The reaction mixture was cooled, diluted with diethyl ether (5 mL) and centrifuged to separate out the supernatant liquid. The process was repeated three times and the combined organic part was evaporated to afford an oily residue. The residue was purified by passing through a short column of silica gel bed and eluting with 2% ethyl acetate–light petroleum as colourless liquid. Although the TLC of the product showed a single spot, the NMR spectra (¹H and ¹³C) revealed a mixture of benzaldehyde and *N*-benzylidenebenzylamine in the ratios 1:10. The peaks for the *N*-benzylidenebenzylamine,³⁹ in the mixture are prominent; ¹H NMR (CDCl₃, 300 MHz): δ/ppm 4.8 (d, *J* = 1.2 Hz, 2H, CH₂), 7.24–7.43 (m, 8H, ArH), 7.76–7.80 (m, 2H, ArH), 8.39 (t, *J* = 1.2 Hz, 1H, CH); ¹³C NMR (CDCl₃, 75 MHz): δ/ppm 65.0, 127.0, 127.9, 128.2, 128.5, 128.6, 130.7, 136.1, 139.2, 162.0.

2.7 Separation and reuse of the MnO₂@AFGNS catalyst

After removing the ethereal washings, the remaining catalyst was washed further with diethyl ether twice to remove any organic material and then dried under vacuum (50 °C at 0.1 mm Hg for 2 h) for further use.

3. Results and Discussion

3.1 Structure and morphology of MnO₂ nanowires

Raman spectral analysis is an important and efficient tool for identifying metal oxide NP owing to their electron–phonon coupling. Thus, for the structural analysis of the composite formed, Raman spectral analysis of MnO₂@AFGNS and AFGNS were carried out which are shown in Fig. 1a. It has been

ARTICLE

Journal Name

reported earlier that the Raman spectrum of MnO_2 shows major features from 500–700 cm^{-1} due to the stretching mode of MnO_6 octahedra.⁴ In the present case also, Raman spectrum of MnO_2 @AFGNS shows a prominent peak at 573 cm^{-1} due to the deformation modes of the Mn–O–Mn chain of MnO_2 with an adjacent weak peak at 508 cm^{-1} and another strong peak at 642 cm^{-1} due to the Mn–O stretching modes which are the characteristic peaks of β - MnO_2 .^{4,40} Another peak was observed at 324 cm^{-1} (inset of Fig. 1a) upon magnification of the spectrum of MnO_2 @AFGNS within the range of 275–350 cm^{-1} . This peak was assigned to the interaction between the metal centre i.e. Mn and $-\text{NH}_2$ which helps in stabilizing the nanowires formed on the AFGNS surface.⁴¹ Along with the characteristic peaks of MnO_2 , peaks at 1345 and 1580 cm^{-1} corresponding to the disordered graphitic lattice (primarily along the edge due to functionalization), D-band and ideal graphitic lattice, G-band of AFGNS were also observed in the spectrum of MnO_2 @AFGNS.⁴² The D/G ratio was ~ 0.25 which was attributed to the functionalization of GNS with $-\text{NH}_2$ group in AFGNS.³⁷ However, along with the peak due to D-band, a smaller hump was observed at 1220 cm^{-1} due to disordered graphitic lattice (A_{1g} symmetry or polyenes) in the Raman spectrum of MnO_2 @AFGNS.⁴² The origin of this peak is

believed to be due to some deformation in the nanosheets of AFGNS owing to self limiting redox reaction between KMnO_4 and AFGNS.^{25,43,44}

The XRD pattern of MnO_2 @AFGNS composite (Fig. 1b) shows the diffraction peaks at $2\theta = 28.4, 37.1, 55.9$ and 58.7° which matched perfectly with the (110), (101), (211) and (220) planes of β - MnO_2 (JCPDS card no. 00-004-0591 having tetragonal symmetry with P42/mnm space group and lattice constant of $a=b=4.44, c=2.89$). Along with the peaks for MnO_2 , peaks at $2\theta = 21.7, 26.4, 44.6$ and 54.4° for the graphitic domain of AFGNS (JCPDS card no 00-008-0415)¹³ was also observed in the XRD pattern of MnO_2 @AFGNS composite. The peak at 21.7° for an inter planar distance of 4.1 Å is due to intercalation of few $-\text{NH}_2$ group in between the nanosheets during synthesis of AFGNS.^{13,37} It is noteworthy to mention here that in case of MnO_2 there is an increase in the ratio of the intensities of (110) and (101) diffraction peaks compared to the conventional value (3.4 versus 1.25 calculated with respect to counts). This indicates the oriented growth of the MnO_2 NP along the (110) plane leading to the formation of nanowires.^{44,45} The analysis of the XRD pattern also shows the presence of an amorphous phase. This was mainly due to the partial oxidation of AFGNS by KMnO_4 as a consequence of the redox reaction as mentioned earlier. Such amorphous phase is typically the characteristic feature of oxidised graphite.⁴⁶

The XPS analysis provides useful information regarding the oxidation state of MnO_2 . The peak position for Mn $2p_{3/2}$ in the high resolution Mn 2p spectrum shown in Fig. 2a was observed at 642.3 eV which indicates that Mn is in +4 oxidation state and it corresponds to β - MnO_2 .²² Further, the peak for Mn $2p_{1/2}$ was observed at 653.8 with 11.5 eV spin energy difference between Mn $2p_{1/2}$ and Mn $2p_{3/2}$ which is consistent with that observed for MnO_2 .²¹ The high resolution O 1s spectrum (Fig. 2b) upon deconvolution by voigt function³⁷

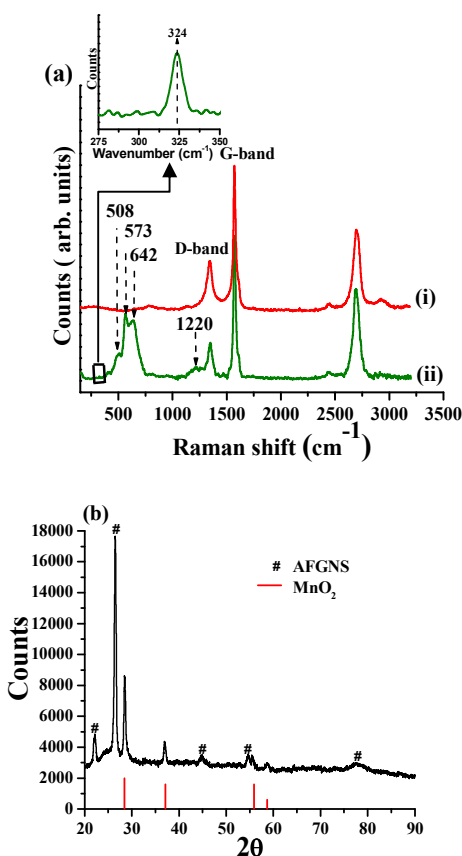


Fig. 1 (a) Raman spectral analysis of (i) AFGNS and (ii) MnO_2 @AFGNS. Marking of the peaks are shown in the body of the figure; (b) XRD pattern of MnO_2 @AFGNS.

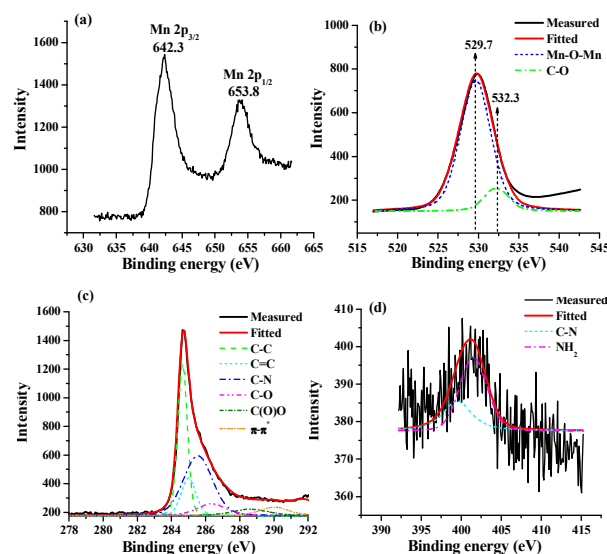


Fig. 2 High resolution (a) Mn 2p, (b) O 1s, (c) C 1s and (d) N 1s XPS spectra of MnO_2 @AFGNS.

shows peaks at 529.7 eV corresponding to Mn–O–Mn and 532.3 eV for the oxygen containing functional groups such as –OH and –COOH.^{47,48} As already mentioned earlier, the KMnO_4 being a very strong oxidizing agent, it creates some –OH and –COOH groups on the surface of AFGNS which is the reason for the origin of the peak at 532.3 eV. The high resolution C 1s spectrum (Fig. 2c) upon deconvolution shows peaks at 284.6, 285, 285.6, 286.3, 288.7 and 290 eV for C–C, C=C, C–N, C–O–H, –COOH and π – π^* for the C–C bond shake up respectively.^{37,49} It is noteworthy here that the peak observed for C–N at 285.6 eV is very prominent in the C 1s spectrum which confirms the presence of – NH_2 group in AFGNS surface.³⁷ The high resolution N 1s spectrum (Fig. 2d) shows peaks at 399.5 eV corresponding to the C–N bond for nitrogen embedded in GNS with three carbon neighbors.¹³ Another peak at 401.4 eV for – NH_2 was also observed which was however at slightly higher binding energy compared to free – NH_2 group due to Mn–N interaction present.^{13,37} As a result, the N 1s electron is present in a more bound condition compared to free state which provides a direct evidence regarding the interaction between the – NH_2 group and MnO_2 . The very low intensity of the N 1s spectrum is attributed to high surface coverage by MnO_2 nanowire thus reducing the extent of their detection.⁵⁰

FESEM analysis helps us to get a clear visual idea about the morphology of MnO_2 @AFGNS composite. FESEM micrograph of AFGNS and MnO_2 @AFGNS powder samples are shown in Fig. 3a and b, respectively. The FESEM micrograph of MnO_2 @AFGNS (Fig. 3b) clearly shows the presence of MnO_2 nanowires on the AFGNS surface in stark contrast to the smooth surface of AFGNS (Fig. 3a). The higher magnification image of the composite (Fig. 3c) showed a similar nanowire structure. However, it is to be noted that on further

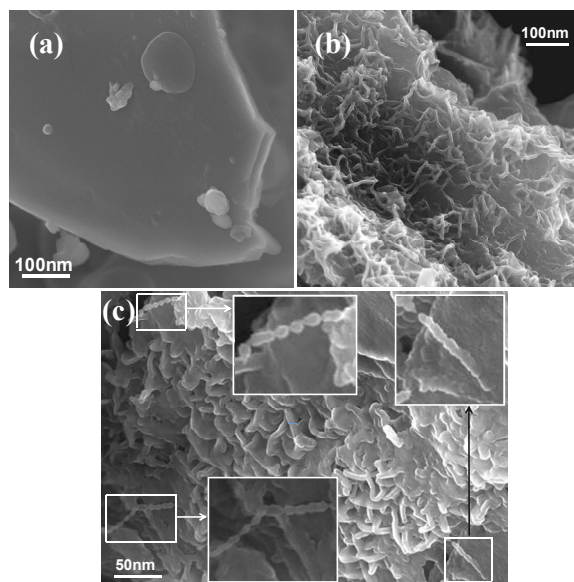


Fig. 3 FESEM micrographs of (a) AFGNS; (b) MnO_2 @AFGNS; (c) higher magnification of MnO_2 @AFGNS with portions magnified in the insets.

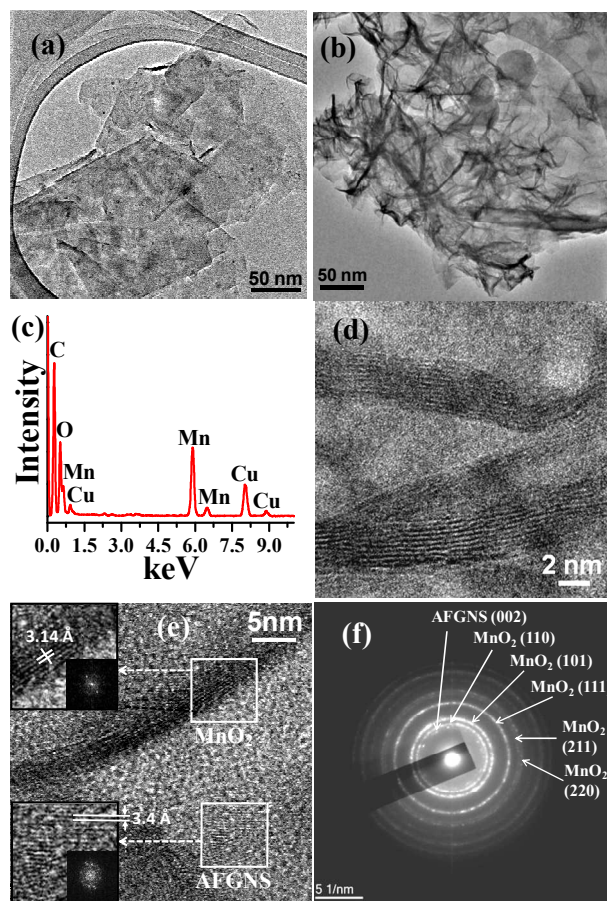


Fig. 4 Bright field TEM image of (a) AFGNS showing few overlapping nanosheets and (b) MnO_2 @AFGNS. (c) EDS spectrum over the region shown in (b) confirming the presence of Mn. Signal of Cu is from the Cu grid used for TEM analysis. (d) and (e) HRTEM images of MnO_2 nanowire on AFGNS. The magnified images of the MnO_2 nanowire and AFGNS and their corresponding FFTs are shown in upper left and lower left insets, respectively in (e). (f) SAED pattern with labelling of different crystalline planes.

magnification of few nanowires, the oriented alignment of the NP in a particular direction was visible. This corroborated with the observation from XRD analysis that preferential growth of the MnO_2 NP along (110) direction leads to the formation of the nanowires.

TEM image shown in Fig. 4 also provides some useful information regarding the morphology of MnO_2 @AFGNS composite. The bright field TEM image of AFGNS (Fig. 4a) shows nanosheets of size around 150 nm with smooth surface. On the other hand, the bright field TEM image of MnO_2 @AFGNS (Fig. 4b) shows the uniform distribution of nanowire like structures on the nanosheet surface. The EDS spectrum (Fig. 4c) over the same region reconfirms the presence of MnO_2 nanowires on the nanosheet surface. The high resolution TEM (HRTEM) image of MnO_2 @AFGNS (Fig. 4d

ARTICLE

Journal Name

and e) shows several MnO₂ nanowire with ~3–4 nm diameter on the surface of AFGNS. The HRTEM of a single MnO₂ nanowire (Fig. 4e) with a portion of the nanowire magnified (upper left inset, Fig. 4e) shows fringes, and the corresponding fast Fourier transform (FFT) exhibit the feature which is a signature of (110) plane of β-MnO₂ with the spacing of $d_{110} = 3.14$ Å. The fringes for the graphitic lattice with interlayer spacing of 3.4 Å was also clearly visible and has been magnified along with the corresponding FFT in the inset of Fig. 4e (lower left). The selected area electron diffraction (SAED) pattern acquired from a lower resolution TEM image (Fig. 4f) shows the characteristic crystalline spots of β-MnO₂ along with the spots for the (002) plane of AFGNS corroborating with the XRD patterns. Thus the FESEM and TEM analysis gives a complete visual microscopic evidence of the presence of MnO₂ nanowires on AFGNS surface in MnO₂@AFGNS composite.

3.2. Plausible mechanism for synthesis of MnO₂@AFGNS

The schematic representation of synthesis of AFGNS, the formation of MnO₂ NP and their oriented growth on AFGNS surface over 48 hrs to form nanowires have been shown in Fig. 5.⁵¹ Formation of the –NO₂ group on GNS surface in the intermediate stage during the synthesis of AFGNS was confirmed from FTIR spectral analysis of –NO₂ functionalized GNS (Fig. S1; ESI[†]). Here prominent peaks at 1390 and 1582 cm^{–1} for the N–O stretching were observed confirming the presence of –NO₂ functional groups on GNS surface.³⁷ Along with the peaks for –NO₂ group, peaks at 2924 and 3444 cm^{–1} for C–H stretching of GNS and O–H stretching of adsorbed moisture were also observed in the FTIR spectrum of –NO₂ functionalized GNS.³⁷ Subsequently the –NO₂ group was reduced to –NH₂ in presence of Na₂S to form AFGNS. This was also confirmed from the corresponding FTIR analysis (Fig. 6(i)) where no peaks due to –NO₂ group was present but instead the peaks due to out of plane N–H bending, C–N stretching and in plane N–H bending were observed at 754, 1027 and 1660 cm^{–1}, respectively due to the –NH₂ groups present on AFGNS surface.^{13,37}

During the synthesis of the composite, the –NH₂ group on

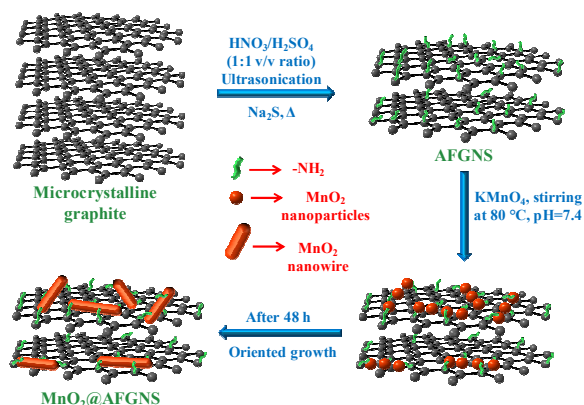


Fig. 5 Schematic representation of synthesis of AFGNS and MnO₂@AFGNS.

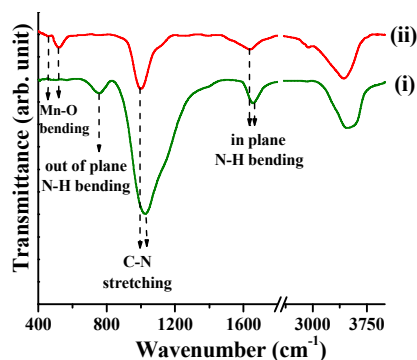


Fig. 6 FTIR spectra of (i) AFGNS and (ii) MnO₂@AFGNS. The marking of the peaks have been shown in the body of the figure.

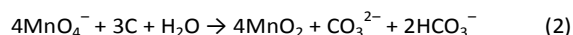
the surface of the AFGNS at the very onset of the reaction help to anchor the permanganate ion (MnO₄[–]),⁵² similar to a previous report by Wang et al for RGO.²⁵ It is a well known phenomenon that KMnO₄ in basic medium undergoes reduction to form MnO₂.⁵³ In the present case also, the –NH₂ group on AFGNS surface creates a weakly basic medium (pH=7.4) and as a result the MnO₄[–] ions gradually get reduced to MnO₂ NP with progress of reaction time. The probable reaction occurring can be represented as:



A preferential growth of the MnO₂ NP along the (110) plane occurs which gives rise to the 1–D nanowire structure.^{25,44} Further, the MnO₂ nanowires already formed act as the seeds to form longer MnO₂ nanowires.²⁵ The MnO₂ nanowires thus formed are attached closely on the AFGNS surface and are stabilized and anchored by the –NH₂ group present on the nanosheet surface.⁵⁴ Evidence of this stabilization was observed from Raman spectra and XPS analysis, as discussed earlier, which was further supported from FTIR spectra analysis. On comparing the FTIR spectra of AFGNS and MnO₂@AFGNS (Fig. 6), a significant decrease in the intensity of the peaks along with a shift in the position from 1027 to 997 cm^{–1} and 1660 to 1636 cm^{–1} for the C–N stretching and in plane N–H bending in MnO₂@AFGNS was observed which was due to the interaction of MnO₂ with the –NH₂ group on AFGNS surface that stabilizes the MnO₂ nanowires.¹³ The absence of the peak at 754 cm^{–1} corresponding to out of plane N–H bending is due to reduction in free –NH₂ group on AFGNS surface as most of the –NH₂ groups are involved in interaction with MnO₂ nanowire and stabilizing them. The FTIR spectrum of MnO₂@AFGNS also shows a peak at 521 cm^{–1} with a shoulder at 462 cm^{–1} which is characteristic for the Mn–O bending vibration of MnO₂ nanowires present on the surface of AFGNS.⁵⁵

It is noteworthy to mention here that, due to the strong oxidizing nature of KMnO₄, a self limiting redox reaction

between AFGNS and KMnO_4 also occurs^{25,43–45} evidence of which was observed in the discussion of Raman, XRD and XPS spectra. This also leads to the synthesis of MnO_2 NP on AFGNS surface. The probable reaction,^{25,43–45} occurring in this case can be represented as:



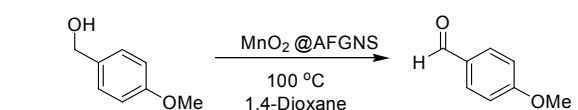
However, from the small D/G ratio observed in Raman spectrum (Fig. 2a), presence of sharp graphitic peak in XRD pattern (Fig. 2b) and lower peak areas for the oxygen containing functional group in the O 1s and C 1s XPS spectra (Fig. 3b,c), it can be inferred that this is not the primary reaction occurring in the present case for the synthesis of MnO_2 . This is because in case of synthesis of MnO_2 only by the redox reaction between KMnO_4 and graphite nanomaterials, extensive damage to the graphitic framework has been observed.⁴⁴ However, as no such severe damage to the graphitic framework has been observed in case of MnO_2 @AFGNS, it indicates the less extent of this reaction. Nonetheless this reaction also contributes towards synthesis of MnO_2 NP.

A control reaction was also carried out to further confirm the anchoring effect of the $-\text{NH}_2$ group in AFGNS by synthesizing MnO_2 with microcrystalline graphite without any functionalization. It was observed from the XRD pattern and the Raman spectrum (Fig. S2 a,b; ESI[†]) that negligible amount of MnO_2 was formed on the surface of the graphite in this case. Some amount of MnO_2 that is formed on the surface of the graphite is by virtue of the self limiting redox reaction as shown in equation 2. But due to the absence of sufficient anchoring groups, the MnO_2 are removed during washing which clearly points out to the importance of the $-\text{NH}_2$ group in AFGNS towards stabilizing and anchoring the MnO_2 , and thus preparation of the MnO_2 @AFGNS composite. Another noteworthy observation was that the MnO_2 formed in this case was of birnessite type (JCPDS card no. 00–018–0802) i.e. δ polymorph which generally possesses 2–D lamellar structure. This points out to the fact that the $-\text{NH}_2$ group in AFGNS plays a role for the formation of 1–D nanowire structure.

3.3 Optimization of the reaction condition for oxidation of benzyl alcohol

The MnO_2 @AFGNS composite having a network of 1–D MnO_2 nanowire on the nearly undamaged graphitic framework of AFGNS surface was subsequently used in as prepared condition for organic oxidation reaction as catalyst. In order to optimize the reaction condition for oxidation of benzyl alcohol, we chose 4–methoxybenzyl alcohol as the model compound and conducted reactions under different loading of the catalyst at varying temperatures. It can be seen from the experimental observations presented in Table 1 that the desired oxidation takes place with 40 mg (0.07 mmol equivalent MnO_2) catalyst mmol^{-1} of the substrate and at 100 °C (entry 3). Reactions carried out in the absence of the catalyst (entry 1), lower concentration of catalyst (entry 2) showed poor performance. On lowering the temperature

Table 1 Optimization of reaction condition using MnO_2 @AFGNS catalyst (7.6 wt% MnO_2).^a



Entry	Catalyst (mg)	Temp. °C	Time (h)	Yield (%) ^b
1	Nil	100	24	trace
2	20	100	20	52
3	40	100	12	82
4	40	80	20	62
5 ^c	40	100	20	34
6 ^d	40	100	12	80
7 ^e	40	100	24	14

[a] 4–methoxybenzyl alcohol (0.5 mmol), 1,4–dioxane (3 mL), reaction carried out under aerobic condition. [b] Isolated yield. [c] Using 1.5 eqv H_2O_2 (30%) under aerobic condition. [d] Under O_2 gas. [e] 4–methoxybenzyl alcohol (0.5 mmol), water (3 mL), reaction carried out under aerobic condition.

(entry 4) or adding additional oxidizing agent (30% H_2O_2) (entry 5), the conversion went down, while carrying out the oxidation in the presence of O_2 did not show any significant change (entry 6). Reaction was also carried out in presence of water which is a green solvent. But the reaction was not successful and only 14% oxidized product (p-anisaldehyde) was isolated (entry 7).

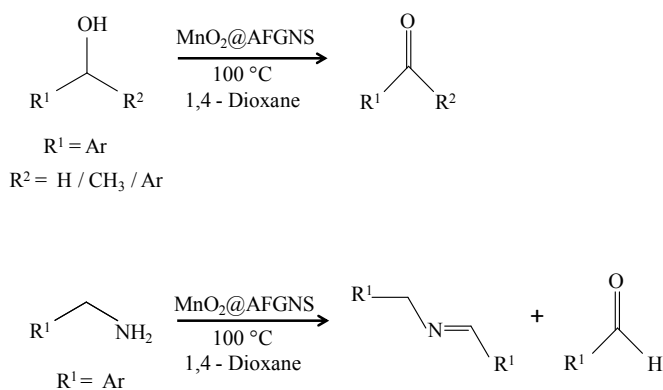
3.4 Oxidation reaction of primary and secondary benzyl alcohols by MnO_2 @AFGNS composite

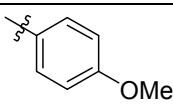
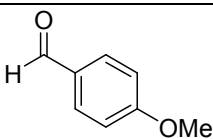
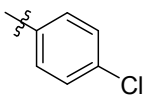
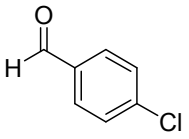
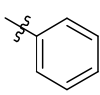
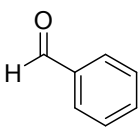
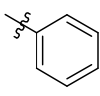
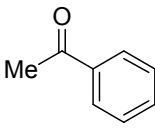
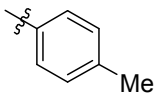
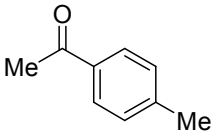
The optimized condition for the catalytic oxidation of benzyl alcohols being confirmed, we explored the general applicability with different primary as well as secondary alcohols. The results are presented in Table 2. The primary benzyl alcohols such as 4–methoxybenzyl alcohol, 4–chlorobenzyl alcohol and benzyl alcohol (Table 2, entries 1–3) underwent smooth oxidation to the corresponding aryl aldehydes with sufficient isolated yields of 82, 79 and 77 %, respectively. Similarly, secondary alcohols such as 1–phenylethanol, 1–(4–methylphenyl)ethanol, 1–(3,4–methoxyphenyl)ethanol, 1–(2–naphthyl)ethanol, 4–(methoxyphenyl)(phenyl)methanol and diphenylmethanol (Table 2, entries 4–9, respectively) yielded aryl alkyl– or diarylketones in good to excellent yields (82–74 %).

We further investigated the efficiency of the catalyst in the oxidation of benzylamine to the *N*–benzylidenebenzylamine. The catalytic oxidation of benzyl amine to imine is also very important as imines are active synthons for the synthesis of industrial materials and biologically active molecules, though, this is a relatively unexplored field.^{56,57} The reaction is believed

RSC Advances

ARTICLE

Table 2 Oxidation of alcohol and amine using MnO₂@AFGNS catalyst.^a

Entry	R ¹	R ²	Time (h)	Product	Yield (%) ^b
1		H	12		82
2		H	12		79
3		H	16		77
4		Me	14		74
5		Me	14		76

Entry	R ¹	R ²	Time (h)	Product	Yield (%) ^b
6		Me	16		81
7		Me	12		82
8		Ph	12		78
9		Ph	14		80
10 ^c		—	12	Mixture of benzaldehyde and imine	Not separated ^d

[a] Reactions carried out: alcohol (0.5 mmol), MnO₂@AFGNS (40 mg, 0.035 mmol equivalent MnO₂), 1,4-dioxane (3 mL) heated at 100 °C in open air. [b] Isolated yield. [c] Reactions carried out: benzylamine (1.0 mmol), MnO₂@AFGNS (40mg, 0.035 mmol equivalent MnO₂) 1,4-dioxane (3 mL) heated at 100 °C in aerobic condition. [d] Conversion is ~ 90% (HPLC), and the ratios of benzaldehyde and *N*-benzylidenebenzylamine were found to be 1:10 (evaluated from ¹H NMR spectrum).

to proceed via initial oxidation of the amine to aldehyde and subsequent condensation with another molecule of amine eventually producing the imine.⁵⁸ On carrying out the oxidation of benzyl amine (Table 2, entry 10) using our catalyst and conditions (40 mg catalyst i.e. 0.035 mmol equivalent MnO₂ mmol⁻¹ of the substrate), we isolated a mixture of benzaldehyde and *N*-benzylidenebenzylamine in the ratios of ~1:10, as evaluated from ¹H-NMR spectrum of the mixture of the products. Thus, from the above mentioned results, it is well established that MnO₂@AFGNS composite can be used as an efficient heterogeneous catalyst for facile oxidations of primary, secondary benzyl alcohols to corresponding carbonyl compounds as well as for the oxidation of benzyl amine to imine. A scheme for the probable overall reaction of catalytic oxidation of alcohol by MnO₂ is shown in Fig. 7a. MnO₂ is known to be very selective towards oxidation of allylic and benzylic alcohol. The oxidation of benzylic alcohol occurs by radical mechanism as proposed by Goldman^{5,35,36} (Scheme 1). As MnO₂ acts as an oxidant for alcohol, during redox reaction it gets reduced to Mn(OH)₂ which undergoes rapid oxidation in air to give back MnO₂.⁵⁹ Thus the composite becomes reusable for application in subsequent reaction cycles. The 1-D nanowire structure is ideal for catalyst application as they have

much higher surface area compared to bulk materials and thin film as a result of which they have more available reactive sites on their surface.¹² However, it is noteworthy here that MnO₂ has low electrical conductivity as mentioned earlier which makes the electronic transfer through them during catalysis unfavourable.¹¹ Here AFGNS plays significant role for their high electrical conductivity owing to nearly undamaged graphitic network. As AFGNS has a planar structure with several nanowires on the surface of the nanosheets, during the redox

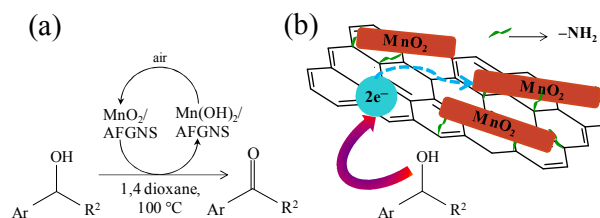
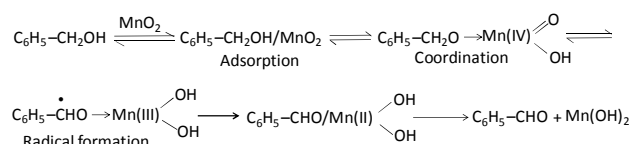


Fig. 7 Schematic representation of (a) the overall reaction of catalytic oxidation of benzylic alcohol in presence of MnO₂ nanowire and (b) participation of AFGNS in enhancing the catalytic efficiency of MnO₂ nanowire.

ARTICLE

Journal Name



Scheme 1. Possible mechanism of oxidation of benzyl alcohol by MnO_2 .

reaction, the e^- from alcohol is transferred to the AFGNS matrix, which conducts it efficiently and rapidly to the different MnO_2 nanowires increasing the catalytic efficiency of the composite as shown in Fig. 7b. As a result, with only 0.07 mmol equivalent MnO_2 per mmol benzyl alcohol, the reaction gives sufficiently high yields in the absence of any other oxidizing agent. Infact, this is the lowest molar equivalent of MnO_2 reported till date to accomplish the reaction with sufficient yield. Otherwise, much excess of MnO_2 (2 mmol equivalent or more per mmol benzyl alcohol) is generally used in order to carry out the oxidation reaction.^{5,33-36} Only very recently, the oxidation of benzyl alcohols by MnO_2 supported on cellulose and wool has been reported in which the reaction was accomplished with a 1:0.1 molar ratio of substrate alcohol to MnO_2 in presence of K_2CO_3 .^{33,34} It is noteworthy here that this oxidation reaction was carried out in presence of an inorganic base (K_2CO_3) which not only acts as an activator for the alcohol but also as a scavenger of water in the organic medium which directly affected the yield of the products. Further, the synthesized MnO_2 reported in ref 34 did not have any well-defined morphology and sufficient crystallinity, and hence in absence of inorganic activator K_2CO_3 yield of product was only 16% and 27% for MnO_2 supported on cellulose³⁴ and wool, respectively.³³ It can be noted here that from green chemistry perspective, avoiding the use of such inorganic activators in the reaction system is a priority of the research community presently.⁶⁰ In the case of MnO_2 @AFGNS, accomplishment of oxidation reactions by much less concentration of MnO_2 is due to the synergistic effect of the highly crystalline 1-D MnO_2 nanowire and AFGNS, as a result of which no extra inorganic activator is required to be added to the reaction medium and the reaction reaches completion with sufficient high yield (82%). In order to understand the contribution of the weakly basic environment created by the $-\text{NH}_2$ group on the AFGNS surface towards the high catalytic efficiency of the composite in the oxidation reaction, we also prepared two other MnO_2 @AFGNS composites with varying quantities of MnO_2 , namely MnO_2 @AFGNS (3.1 wt%) and MnO_2 @AFGNS (6 wt%) with 3.1 and 6 wt% of MnO_2 in the composite, respectively. We employed both materials in the catalytic oxidation of 4-methoxybenzyl alcohol using the same MnO_2 content (0.07 mmol equivalent MnO_2 per mmol benzyl alcohol) under similar conditions. As presented in Table S1 (ESI[†]), MnO_2 @AFGNS (6 wt%) worked quite efficiently, while further lowering of MnO_2 loading, i.e. MnO_2 @AFGNS (3.1 wt%), led to relatively poor yield of the oxidized product. This suggests that the $-\text{NH}_2$ group on the AFGNS surface might

render its basicity to a certain extent and there is an optimization between the loading of MnO_2 and the surface $-\text{NH}_2$ group in AFGNS for carrying out the reaction efficiently. Thus on the basis of the above discussion, it is believed that MnO_2 @AFGNS can act as a very efficient catalyst for organic oxidation reactions.

3.5 Reusability of the catalyst and characterization of the recovered catalyst

The reusability efficiency of a catalyst is of significant importance from industrial point of view. The more reusable a catalyst is, the more is its potential for extensive industrial applications. Thus to check the reusability of MnO_2 @AFGNS catalyst in subsequent cycles of reaction, the composite was separated by the method mentioned in section 2.7. The presence of the AFGNS matrix makes the MnO_2 @AFGNS a heterogeneous catalytic system which makes them easily separable from the reaction medium. The recycling reactions were carried out with 4-methoxybenzyl alcohol and the yield was calculated in 3 subsequent reaction cycles. The isolated yield was found to be appreciable up to 3 cycles tested, the yield is decreasing from 82% in the first cycle to 80% in the second cycle and finally to 76% in the third cycle (Fig. S3; ESI[†]). This observation confirms the heterogeneous nature of the MnO_2 @AFGNS catalyst and asserts of the fact that the catalyst is potentially recyclable with sufficient reusability capacity.

The MnO_2 @AFGNS catalyst was recovered from the reaction mixture after every cycle and characterized to check the stability of the composite in the reaction condition. Raman spectral analysis of the recovered composite after every cycle of reaction (3 consecutive cycles) and the starting MnO_2 @AFGNS composite (Fig. 8a) showed similar peaks indicating the unchanged oxidation state of the metal oxide. The main peaks at 573 and 642 cm^{-1} for the deformation mode of Mn–O–Mn chain and the Mn–O stretching mode of $\beta\text{-MnO}_2$ ^{4,40} was clearly observed in the composite sample up to 3 cycles of organic reaction which confirms the stability of the composite and that no change of MnO_2 occurred during the course of the reaction. The XRD analysis as shown in Fig. 8b for the composite recovered after each cycle of catalytic reaction also supported this observation. The peaks for (110), (101), (211) and (222) planes of $\beta\text{-MnO}_2$ were observed in all the three set of samples of composite after the 3 reaction cycles along with the peaks for AFGNS as discussed earlier. However, an interesting observation in this context was that the ratio of the intensity of the peaks (calculated with respect to counts) of the (110) and (101) planes of MnO_2 changed from 3.4 before catalysis to 2.7, 2.3 and finally 1.8 after first, second and third cycle of catalysis respectively. This indicates deterioration in the nanowire structure of MnO_2 which subsequently leads to a slight decrease in the yield of the product in the third cycle (~6%) of the catalytic reaction. To confirm the above mentioned observation, TEM analysis of the catalyst recovered after the third cycle was performed (Fig. S4; ESI[†]). From the bright field TEM image, it was seen that although there are nanowire structures visible on the AFGNS surface, some agglomerated NP (marked in the inset) are also

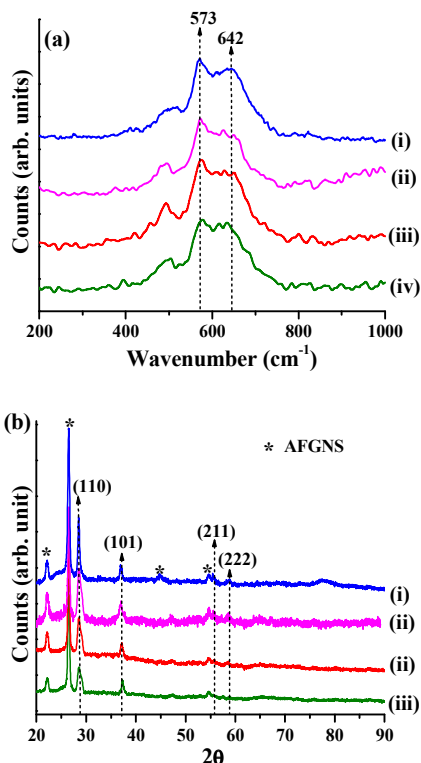


Fig. 8 (a) Raman spectra and (b) XRD patterns of (i) MnO_2 @AFGNS before catalysis and after the first (ii), second (iii) and third (iv) cycles of catalysis.

observed corroborating the observation from XRD analysis. However, the extent of decrease in the catalytic efficiency for this deterioration in structure is comparatively less even after 3 cycles as the active surface of MnO_2 is still available for the reaction. Thus the MnO_2 @AFGNS composite being a cheap and cost effective functional material can have efficient applications in the field of organic catalysis and other related systems.

4. Conclusion

MnO_2 nanowires have been synthesized on amine functionalized graphite nanosheet support to prepare MnO_2 @AFGNS composite. The $-\text{NH}_2$ group on the surface of nanosheet helps simultaneously creating a mild reducing environment to reduce permanganate to MnO_2 , followed by anchoring the MnO_2 nanoparticles on its surface and oriented growth to form nanowire structures. A mechanism has been proposed for the entire synthesis of MnO_2 nanowire anchored AFGNS composite. This composite has been successfully used in catalytic oxidation of primary and secondary benzyl alcohols to corresponding carbonyl compounds selectively in the absence of any other oxidizing and activating agent with significantly high yield. Further, oxidation of amine to imine and aldehyde has also been performed demonstrating the

versatility of the composite as the catalyst in organic oxidation reactions. Straightforward preparative method for the MnO_2 @AFGNS nanocomposite with oriented growth of MnO_2 nanowires, oxidation of benzyl alcohol and amine using a very low concentration of equivalent MnO_2 as the catalyst, ease of recovery and reusability for three runs tested are notable features for the present work. The synergistic effect of MnO_2 nanowire and AFGNS sheet i. e. electron rich surface of AFGNS is presumably enhancing the process of electron transfer by MnO_2 during catalysis that has been explained to be the cause of huge increase in catalytic efficiency of the composite. Thus, the MnO_2 @AFGNS composite can be used as a cheap high potential catalyst in organic oxidation reactions

Acknowledgements

AC and DS thank CSIR, India for providing fellowships.

References

- 1 R. C. Larock, *Comprehensive Organic Transformations*, Wiley-VCH, New York, NY, 1989, 604.
- 2 A. K. Mukhopadhyay, *Industrial Chemical Cresols and Downstream Derivatives*, CRC press, 2004, 66.
- 3 D. V. Bavykin, A. A. Lapkin, S. T. Kolaczkowski and P. K. Plucinski, *Appl. Catal. A*, 2005, **288**, 175.
- 4 S. Liang, F. Teng, G. Bulgan, R. Zong and Y. Zhu, *J. Phys. Chem. C*, 2008, **112**, 5307.
- 5 T. Gabriel and M. Fernandez, *Oxidation of Alcohols to Aldehydes and Ketones*, Springer, USA, 2006, 290.
- 6 M. A. Hasan, M. I. Zaki, L. Pasupulety and K. Kumari, *Appl. Catal. A*, 1999, **181**, 171.
- 7 F. Cheng, J. Shen, W. Ji, Z. Tao and J. Chen, *ACS Appl. Mater. Interfaces*, 2009, **1**, 460.
- 8 L. Blackburn, X. Wei and R. J. K. Taylor, *Chem. Commun.*, **1999**, 1337.
- 9 Z. Zhang, F. Wang, M. Wang, S. Xu, H. Chen, C. Zhang and J. Xu, *Green Chem.*, 2014, **16**, 2523.
- 10 Z. Lu, K. Lin and J. Gana, *Environ. Pollut.*, 2011, **159**, 2546.
- 11 F. Cheng, Y. Su, J. Liang, Z. Tao and J. Chen, *Chem. Mater.*, 2010, **22**, 898.
- 12 W. Zhang, Z. Yang, X. Wang, Y. Zhang, X. Wen and S. Yang, *Catal. Commun.*, 2006, **7**, 408.
- 13 A. Chakravarty, K. Bhowmik, A. Mukherjee and G. De, *Langmuir*, 2015, **31**, 5210.
- 14 P. V. Kamat, *J. Phys. Chem. Lett.*, 2010, **1**, 520.
- 15 J. Yan, Z. Fan, T. Wei, Z. Qie, S. Wang and M. Zhang, *Mater. Sci. Eng. B*, 2005, **151**, 174.
- 16 R. Nie, J. Shi, S. Xia, L. Shen, P. Chen, Z. Hou and F. S. Xiao, *J. Mater. Chem.*, 2012, **22**, 18115.
- 17 A. Yu, H. W. Park, A. Davies, D. C. Higgins, Z. Chen and X. Xiao, *J. Phys. Chem. Lett.*, 2011, **2**, 1855.
- 18 S. Kumari, A. Shekhara and D. D. Pathak, *RSC Adv.*, 2014, **4**, 61187.
- 19 A. K. Sinha, M. Pradhan and T. Pal, *J. Phys. Chem. C*, 2013, **117**, 23976.
- 20 A. M. Morales and C. M. Lieber, *Science*, 1998, **279**, 208.
- 21 Y. Zheng, Q. Du, M. He, Z. Deng and X. Liu, *Micro Nano Lett.*, 2012, **7**, 778.
- 22 Y. Zheng, Q. Du, M. He, Z. Deng and X. Liu, *J. Mater. Chem.*, 2012, **22**, 23525.
- 23 Y. Yu, B. Zhang, Y. B. He, Z. D. Huang, S. W. Oh and J. K. Kim, *J. Mater. Chem. A*, 2013, **1**, 1163.

ARTICLE

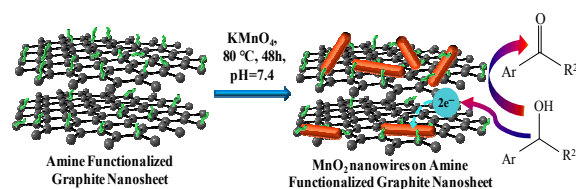
Journal Name

- 24 K. Dai, L. Lu, C. Liang, J. Dai, Q. Liu, Y. Zhang, G. Zhu and Z. Liu, *Electrochim. Acta*, 2014, **116**, 111.
- 25 L. Wang, D. Da Deng and K. Y. Simon Ng, *J. Mater. Sci.*, 2013, **48**, 6410.
- 26 P. Tang, L. Han and L. Zhang, *ACS Appl. Mater. Interfaces*, 2014, **6**, 10506.
- 27 H. Yang, J. Jiang, W. Zhou, L. Lai, L. Xi, Y. M. Lam, Z. Shen, B. Khezri and T. Yu, *Nanoscale Res. Lett.*, 2011, **6**, 531-1.
- 28 Z. S. Wu, W. Ren, D. W. Wang, F. Li, B. Liu and H. M. Cheng, *ACS Nano*, 2010, **4**, 5835.
- 29 Q. Zhang, Y. Q. He, X. G. Chen, D. H. Hu, L. J. Li, T. Yin and L. L. Ji, *Chin. Sci. Bull.*, 2011, **56**, 331.
- 30 M. Epifani, G. De, A. Licciulli and L. Vasanelli, *J. Mater. Chem.*, 2001, **11**, 3326.
- 31 R. Jothiramalingam, B. Viswanathan and T. K. Varadarajan, *J. Mol. Catal. A: Chem.*, 2006, **252**, 49.
- 32 L. C. Wang, L. He, Q. Liu, Y. M. Liu, M. Chen, Y. Cao, H. Y. He and K. N. Fan, *Appl. Catal. A*, 2008, **344**, 150.
- 33 A. Shaabani, Z. Hezarkhani and E. Badali, *RSC Adv.*, 2015, **5**, 61759.
- 34 A. Shaabani, Z. Hezarkhani and S. Shaabani, *RSC Adv.*, 2014, **4**, 64419.
- 35 J. D. Lou, J. Ge, X. N. Zou, C. Zhang, Q. Wang and Y. C. Ma, *Oxid. Commun.*, 2011, **34**, 361.
- 36 J. D. Lou, X. L. Lu, L. H. Huang, Q. Wang and X. N. Zou, *Synth. React. Inorg., Metal–Org., Nano–Metal Chem.*, 2011, **41**, 1342.
- 37 A. Chakravarty, K. Bhowmik, G. De and A. Mukherjee, *New J. Chem.*, 2015, **39**, 2451.
- 38 M. Iinuma, K. Moriyama and H. Togo, *Tetrahedron*, 2013, **69**, 2961.
- 39 G. Chu and C. Li, *Org. Biomol. Chem.*, 2010, **8**, 4716.
- 40 F. Buciuman, F. Patcas, R. Craciun and D. R. T. Zahn, *Phys. Chem. Chem. Phys.*, 1999, **1**, 185.
- 41 K. Nakamoto, *Infrared and Raman Spectra of Inorganic and Coordination Compounds*, 4th edition, Wiley–Interscience Publication, USA, 1986, 192.
- 42 A. Sadezky, H. Muckenhuber, H. Grothe, R. Niessner and U. Pöschl, *Carbon*, 2015, **43**, 1731.
- 43 H. Y. Chu, Q. Y. Lai, L. Wang, J. F. Lu and Y. Zhao, *Ionics*, 2010, **16**, 233.
- 44 Z. Fan, J. Yan, T. Wei, L. Zhi, G. Ning, T. Li and F. Wei, *Adv. Funct. Mater.*, 2011, **21**, 2366.
- 45 J. Wang, Q. Chen, B. Hou and Z. Peng, *Eur. J. Inorg. Chem.*, 2004, **2004**, 1165.
- 46 G. Eda, J. Ball, C. Mattevi, M. Acik, L. Artiglia, G. Granozzi, Y. Chabal, T. D. Anthopoulos and M. Chhowalla, *J. Mater. Chem.*, 2011, **21**, 11217.
- 47 J. Qu, L. Shi, C. He, F. Gao, B. Li, Q. Zhou, H. Hu, G. Shao, X. Wang and J. Qiu, *Carbon*, 2014, **66**, 485.
- 48 U. Zielke, K. J. Hutter and W. P. Hoffman, *Carbon*, 1996, **34**, 983.
- 49 C. Moreno–Castilla, M. V. López–Ramón and F. Carrasco–Marina, *Carbon*, 2000, **38**, 1995.
- 50 Y. W. Fen and M. Y. W. Mahmood, *J. Mater. Sci. Eng. B*, 2011, **1**, 584.
- 51 It is to be noted that from the Fig. 5 it should not be confused that the MnO₂ NP and nanowires are present in between the sheets as no increase in interplanar distance of AFGNS was observed. The MnO₂ NP and nanowires are present on the upper surface and overlapped region of the nanosheets which has been shown schematically in Fig. 5.
- 52 A. L. Harihar, M. R. Kumbhavi and S. T. Nandibewoor, *Indian J. Chem.*, 2009, **39A**, 769.
- 53 T. Moeller, *Inorganic Chemistry: An Advanced Textbook*, Asia Publishing House, India, 1952.
- 54 T. Takashima, K. Hashimoto and R. Nakamura, *J. Am. Chem. Soc.*, 2012, **134**, 18153.
- 55 H. Y. Ju and L. W. Shan, *J. Inorg. Mater.*, 2013, **28**, 341.
- 56 S. I. Murahashi, *Angew. Chem. Int. Ed. Engl.*, 1995, **34**, 2443.
- 57 N. Uematsu, A. Fujii, S. Hashiguchi, T. Ikariya and R. Noyori, *J. Am. Chem. Soc.*, 1996, **118**, 4916.
- 58 H. Huang, J. Huang, Y. M. Liu, H. Y. He, Y. Cao and K. N. Fan, *Green Chem.*, 2012, **14**, 930.
- 59 P. K. Nayak, S. Devaraj and N. Munichandraiah, *Electrochem. Solid St.*, 2010, **13**, 29.
- 60 M. Mahyari, M. S. Laeini and A. Shaabani, *Chem. Commun.*, 2014, **50**, 7855.

RSC Advances

ARTICLE

Graphical Content Entry



MnO₂ nanowires were synthesized on amine functionalized graphite nanosheet and excellent catalytic efficiency of as-prepared composite towards organic oxidation reactions was demonstrated.